Optical Engineering 48(10), 105601 (October 2009)

Phase unwrapping error reduction framework for a multiple-wavelength phase-shifting algorithm

Song Zhang, MEMBER SPIE
Iowa State University
Department of Mechanical Engineering
Virtual Reality Applications Center
Human Computer Interaction
Ames, Iowa 50011
E-mail: song@iastate.edu

Abstract. We address a framework to reduce the unwrapping errors of the measurement system using a digital multiple-wavelength phase-shifting algorithm. In particular, the following framework is proposed: (1) smooth the raw phase by smoothing the sine and cosine images of the phase computation of the inverse tangent function; (2) locate and remove the incorrectly unwrapped points by the monotonicity condition of the phase map; (3) obtain the unwrapped phase map for the shortest wavelength without smoothing; (4) detect holes and fill them to preserve as much useful information as possible. Experiments demonstrated that the proposed framework significantly alleviated the measurement errors caused by the phase noise. [DOI: 10.1117/1.3251280]

Subject terms: structured light; phase shifting; phase unwrapping; multiple wavelength; phase error.

Paper 090501 received Jul. 6, 2009; accepted for publication Aug. 24, 2009; published online Oct. 23, 2009.

1 Introduction

Over the years, phase-shifting algorithms are widely used for 3-D profile measurement due to their measurement speed and accuracy. For these methods, a phase unwrapping algorithm is usually necessary to obtain continuous phase maps. Typically, the surface smoothness is assumed for the phase unwrapping step—namely, the object surface height changes cannot be beyond 1/4 of the wavelength used. However, in numerous situations, this requirement is very difficult to satisfy, and objects with step-height exist everywhere, especially in the manufacturing field. Therefore, determining how to measure these objects using phase-shifting methods is vital, with broad applications including manufacturing, medical sciences, and computer sciences.

The limitations of a single-wavelength phase algorithm are significantly alleviated if a two- or multiple-wavelength technique is employed. Especially when a multiple-wavelength technique is utilized, the measurement can be performed point by point without any spatial phase unwrapping; therefore, the step-height is not a problem at all. Over the years, extensive research has been conducted on two- or multiple-wavelength phase-shifting techniques[1–14] and temporal phase unwrapping.[15,16] All these efforts were intending to measure the step-height object or alleviate the limitations of phase unwrapping.

In general, for a phase-shifting technique, the longer the wavelength used, the larger the phase noise induced. The phase noise is proportional to the wavelength of the fringe image used. To completely eliminate the step-height problems, a multiple-wavelength phase-shifting (MWPS) technique chooses the longest wavelength fringe to cover the whole projection area, but its drawback is that the noise might be too large to recover the signal. In comparison with a single-wavelength phase-shifting technique that uses a shorter wavelength, this technique is more sensitive to phase noise. Therefore, the noise plays a significantly larger role for the multiple-wavelength phase shifting technique. Reducing the phase noise is vital for the success of this technique to measure objects with larger surface reflectivity variations. In this research, we propose a framework to alleviate the problem caused by the phase noise of the MWPS. It should be noted that *wavelength* as defined in this paper is different from that defined in physics. The wavelength here indicates the spatial width of the fringe stripes, i.e., number of pixels per fringe stripe. Experiments are presented to demonstrate that the proposed frame significantly alleviated the measurement phase errors caused by the phase noise.

Section 2 introduces the multiple-wavelength phase-shifting algorithm. Section 3 explains the detailed procedures of the proposed technique. Section 4 introduces the system setup. Section 5 shows some experimental results, and Sec. 6 summarizes the work.

2 Multiple-Wavelength Phase-Shifting Algorithm

Phase-shifting algorithms are widely used due to their measurement speed and surface noncontact nature. For a single-wavelength phase-shifting algorithm, a number of fringe images having the same wavelength (λ) with certain phase shift are used to obtain the phase ϕ. For example, three fringe images of a three-step phase-shifting algorithm with a phase shift of $2\pi/3$ can be represented as

$$I_k(x,y) = I'(x,y) + I''(x,y)\cos\left[\frac{2\pi h(x,y)}{\lambda} + \frac{2k\pi}{3}\right], \qquad (1)$$

where $k=0,1,2$, $I'(x,y)$ is the average intensity, $I''(x,y)$ the intensity modulation, and $h(x,y)$ is the spacial distance. The phase to be solved for is

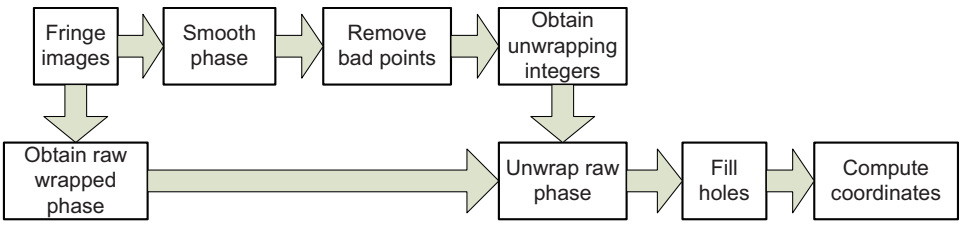

Fig. 1 Proposed framework to reduce the noise influence for the MWPS algorim.

$$\phi(x,y) = \frac{2\pi h(x,y)}{\lambda}. \tag{2}$$

In general, $\phi(x,y)$, ranges from $-\pi$ to $+\pi$ by direct calculation of the fringe images. The real phase, $\Phi(x,y)$, should be continuous as a function of $\phi(x,y)$:

$$\Phi(x,y) = 2\pi m(x,y) + \phi(x,y), \tag{3}$$

where $m(x,y)$ are integers. If only a single fringe stripe is used, $\phi(x,y)=\Phi(x,y)$ and $m(x,y)\equiv 0$, and no phase unwrapping is necessary. However, if multiple fringe stripes are used, $m(x,y)$ are not always zeros, and a phase-unwrapping algorithm is required to remove the 2π discontinuities by detecting the correct integers, $m(x,y)$, from the neighborhood points.[17] Although numerous phase-unwrapping algorithms have been proposed, none can 100% correctly retrieve the true phase value especially for step-height objects.

For a multiple-wavelength phase-shifting (MWPS) algorithm, different wavelengths are used to measure step-height. For each wavelength, the phase-shifting algorithm is employed to obtain the phase. In this research, we use the wavelength $\lambda_k = N\lambda_{k+1)}$, $k=1,2,3,\ldots$. Assume that the projector has a resolution of $W\times H$ and the fringe stripes are vertical. If we choose $\lambda_1 = W$, there is no need for phase unwrapping for this phase map because the single fringe covers the whole area—that is,

$$\Phi_1(x,y) = \phi_1(x,y). \tag{4}$$

Here, $\Phi_1(x,y)$ represents the unwrapped phase, and $\phi_1(x,y)$ the wrapped phase.

For the phase $\phi_2(x,y)$, $m_s(x,y)$ are not always zeros and need to be detected. Because $\lambda_1 = N\lambda_2$, we have $\Phi_2 = N\Phi_1$. Combining with Eq. (3),

$$m_2(x,y) = \text{Round}\left[\frac{N\Phi_1(x,y)}{2\pi} - \frac{\phi_2(x,y)}{2\pi}\right]. \tag{5}$$

Here operator Round$[X]$ is to compute the closest integer value of X. This means that the wrapped phase, $\phi_2(x,y)$, can be unwrapped pixel by pixel by referring to the unwrapped longer wavelength phase $\Phi_1(x,y)$.

Once $\Phi_2(x,y)$ is obtained, we can use it to correct $\Phi_3(x,y)$. In general, for $\lambda_k = \lambda_{k-1}/N$,

$$m_k(x,y) = \text{Round}\left[\frac{N\Phi_{k-1}(x,y)}{2\pi} - \frac{\phi_k(x,y)}{2\pi}\right], \tag{6}$$

and

$$\Phi_k(x,y) = 2\pi m_k(x,y) + \phi_k(x,y). \tag{7}$$

Since the unwrapped phase is obtained pixel by pixel without accessing its neighborhood pixels, this technique can be used to measure surface profile with arbitrary step-height, and the measurement noise is close to that using a single-wavelength phase-shifting technique with the shortest wavelength. Because only integers are to be obtained using the longer wavelength, the noise of the longer wavelength will not significantly affect the measurement. However, our experiments found that for weak signals, this would be problematic. This paper addresses a framework to handle this problem.

3 Framework

The proposed framework is shown in Fig. 1. The processing procedures are:

1. Apply Gaussian filtering first to remove the random noise.
2. Detect the incorrectly unwrapped points based on phase monotonicity.
3. Unwrap the shortest wavelength phase without smoothing for the final measurement.
4. Detect holes that should be filled and fill them.
5. Last, use the phase to calculate the coordinates.

The details of each step are described in the following sections.

3.1 *Phase Noise Reduction—Gaussian Smoothing*

Random phase noise is one of the largest error sources contributing to the incorrectly calculated integers, $m(x,y)$. It can be shown that the longer the wavelength, the larger the phase noise. In this section, without losing generosity, the longest wavelength is used to illustrate the noise effect.

The signal-to-noise ratio (SNR) of the fringe images plays a key role for the phase noise. The SNR is most significantly affected by the ambient light, the sampling bits number of the camera, the brightness of the fringe images, and the sensor noise. The SNR is usually reflected by the value of data modulation, $\gamma(x,y)=I''(x,y)/I'(x,y)$, for a phase-shifting algorithm, with 1 being the best when the ambient light is always 0. However, in practice, it is very difficult to ensure such measurement conditions. Moreover,

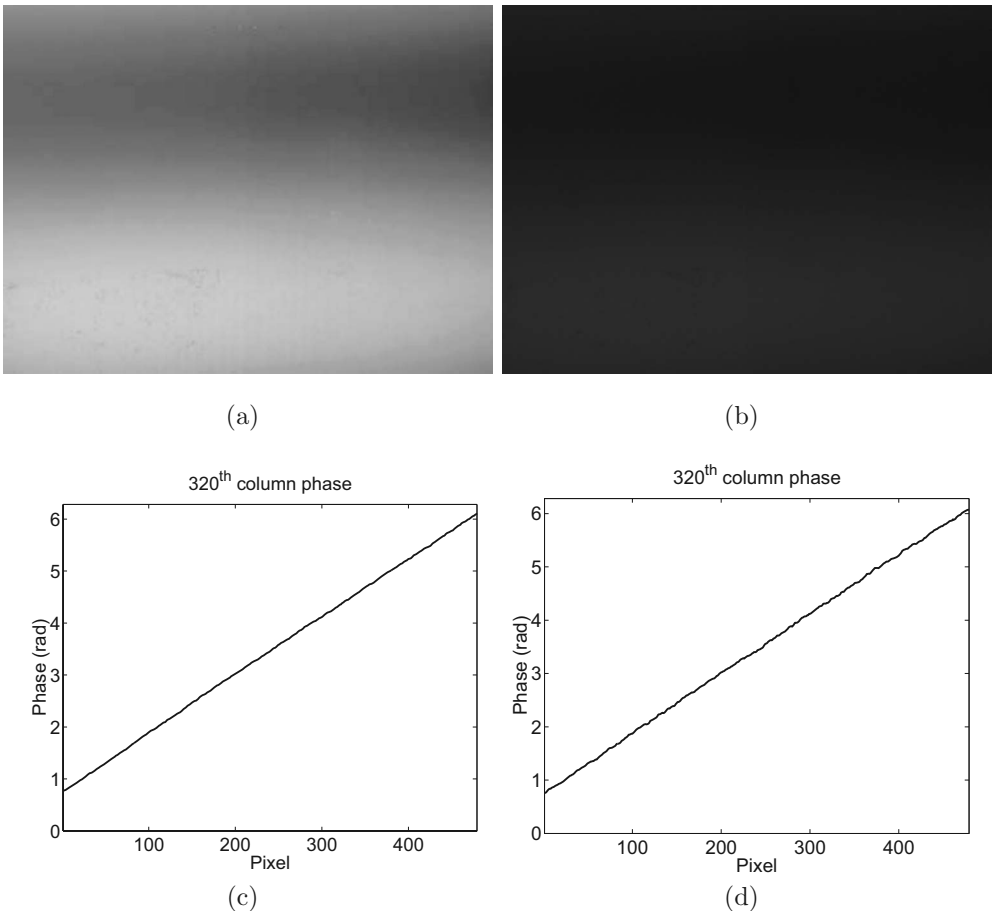

Fig. 2 Comparison between the brighter fringe images and darker fringe images under the same room lighting condition, but with different camera aperture. (a) Brighter fringe image; (b) darker fringe image; (c) cross section of phase for brighter fringe image; and (d) cross section of the phase for darker fringe image.

considering the digital sampling of the camera, the brighter the fringe images, the better the quality of data. If the surface reflectivity varies across the surface, it also affects the measurement.

To analyze the effect of noise, we took two sets of fringe images under the same room lighting condition. The only difference is their overall brightness by adjusting the aperture of the camera during data acquisition. Figure 2 shows one of the longest wavelength fringe images for each set. Figure 2(a) is the brighter fringe image, and Fig. 2(b) shows its corresponding darker fringe image where the fringe is barely seen. The corresponding phases for this wavelength are shown in Fig. 2(c) and 2(d), respectively. The phase noise is larger for the darker fringe images. To visualize the phase noise better, the slope of the phase is removed, and the noise is plotted in Fig. 3. This figure clearly shows that the dimmer fringe phase error is already approximately ± 0.18 rad. From Eq. (5), the phase error will be multiplied by an integer number $N(N=2,3,\ldots)$. For the minimum $N=2$, the phase error that affects the final phase unwrapping is already ± 0.36 rad, which is approximately $0.72/(2\pi)=11.5\%$. For high-quality measurement, this error has to be reduced.

Because the noise of the phase is random, a Gaussian smoothing filter can be used to reduce it. In general, a 2-D Gaussian filter can be written as

$$G(x,y)=\frac{1}{a}\exp\left[\frac{(x-x_0)^2+(y-y_0)^2}{2\pi\sigma^2}\right], \tag{8}$$

where $a=\int_x\int_y \exp\{[(x-x_0)^2+(y-y_0)^2]/(2\pi\sigma^2)\}\mathrm{d}x\ \mathrm{d}y$. (x_0,y_0) is the center of the filter, and σ is the standard deviation. The wrapped phase is usually computed using an inverse tangent function:

$$\phi(x,y)=\tan^{-1}\left[\frac{N(I_k)}{D(I_k)}\right], \tag{9}$$

where $N(I_k)$ is the numerator as a function of the fringe images, and $D(I_k)$ is the denominator as a function of the fringe images. The Gaussian smoothing is applied to the numerator and the denominator separately:

$$\tilde{N}(I_k)=N[I_k(x,y)]\star G(x,y),$$

and

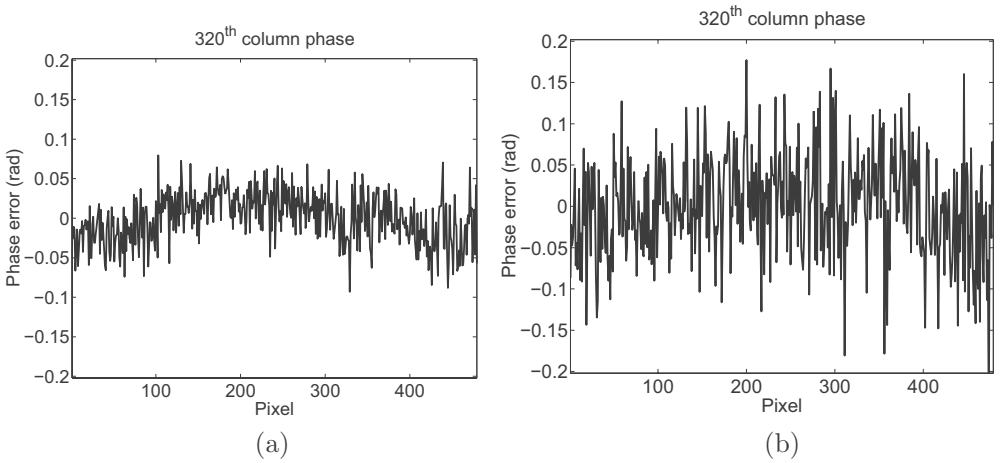

Fig. 3 Cross sections of phase noise for different brightness fringe images. (a) Brighter fringe images; (b) darker fringe images.

$$\tilde{D}(I_k) = D[I_k(x,y)] \star G(x,y),$$

where operator $\star$ represents convolution, and $\tilde{X}$ means the smoothed value of X. (This notation holds for the remaining discussion.) It can be shown that this operation removes only the random phase noise without introducing phase errors. After smoothing, the phase becomes

$$\tilde{\phi}(x,y) = \frac{\tilde{N}[I_k(x,y)]}{\tilde{D}[I_k(x,y)]}.$$

By applying a 7×7 Gaussian filter for the numerator and the denominator, the phase is plotted in Fig. 4(a) for the phase shown in Fig. 3(b). The random phase noise is significantly reduced. The difference between the smoothed phase and the raw phase is plotted in Fig. 4(b), which comprises only random noise. The most significant noise has been reduced to approximately ± 0.025 rad, which is more than 7 times smaller. Moreover, from this example, it can been seen that the denoising does not affect the major phase value, it only reduces the random noise, as expected.

3.2 *Incorrectly Unwrapped Points Detection—Phase Monotonicity*

The denoising step reduces only the random noise, for some surfaces with lower SNR, especially when the surface reflectivity varies drastically across the surface. For the low surface reflectivity points, the fringe is barely visible, and the phase noise is so significant that the previous step cannot completely eliminate its influence. And some points might still be incorrectly unwrapped. Thus, those bad points have to be detected and removed.

From the configuration of the system, it is clear that the phase is monotonic along the direction perpendicular to the fringe stripes. These constraints will help detect the incorrectly unwrapped points line by line. Assuming that the fringe stripes are horizontal, vertically the phase should be monotonically increasing (or decreasing). Assuming that the phase is increasing, we have

$$\tilde{\Phi}(x,y) < \tilde{\Phi}(x,y+1).$$

Therefore, any point that does not satisfy this condition should be regarded as an incorrectly unwrapped point.

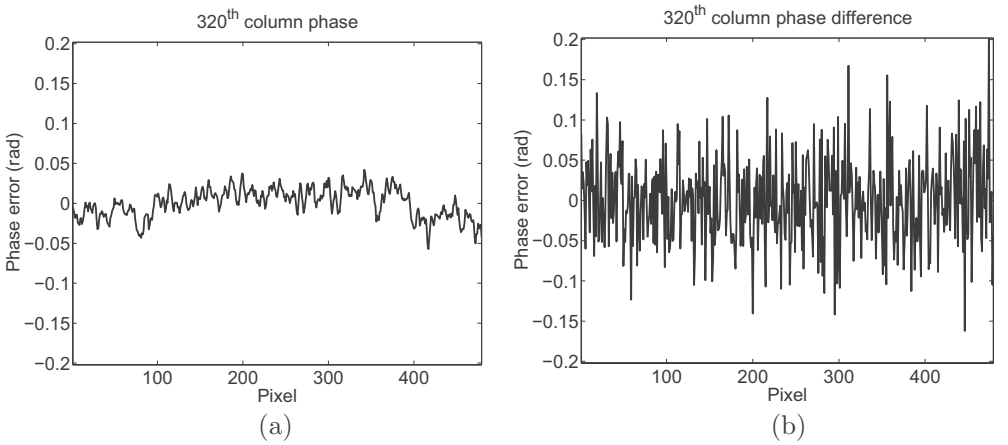

Fig. 4 The smoothing influence on the phase error. (a) Smoothed phase; (b) difference between the smoothed phase and the original phase.

3.3 *Raw Unwrapped Phase Recovering*

The Gaussian smoothing is not desirable for the final measurement, since it removes the details. If the long-wavelength fringe images are used, the random noise is significant, and filtering improves the measurement. However, for shorter wavelengths, the random phase noise is not so dramatic, and the smoothing actually removes a lot of details. Therefore, the raw phase data without smoothing needs to be preserved. In this research, the correct integers, $\tilde{m}_K(x,y)$, are obtained using the smoothed phase but are applied to the raw wrapped phase to achieve the original unwrapped phase data—that is,

$$\Phi_K(x,y) = \phi_K(x,y) + \tilde{m}_K(x,y) \times 2\pi.$$

3.4 *Useful Information Preservation—Hole Detection and Filling*

To alleviate the effect of the low SNR points, a higher threshold (γ_h) is desired for the phase calculation. But a lower threshold (γ_l) is required for the final measurement to preserve as much useful information as possible. This is a dilemma! In this research, we propose a method called *hole detection and filling* to provide a solution.

Assume that for the higher threshold, γ_h, the background points are marked by a mask $M_h(x,y)=0$, and for the lower threshold, γ_l, the background points are marked by the mask $M_l(x,y)=0$. The hole detection and filling is to find points that satisfy $M_l(x,y)\neq 0$ and $M_h(x,y)=0$.

For these points, we first find the single individual connected component to form a single hole. For each hole, the boundary ($x_0 \leqslant x \leqslant x_1$, $y_0 \leqslant y \leqslant y_1$) is found, and a subimage with ($[x_0-1:x_1+1, y_0-1:y1+1]$) is formed. This subimage is then unwrapped using a conventional phase-unwrapping algorithm to obtain the unwrapped phase Φ_s^l (Ref. 18). Once this subimage is unwrapped, within this subimage, for points that have already been unwrapped using the multiple-wavelength algorithm, we take the difference:

$$\delta\Phi = [\Phi_s^l(x,y) - \Phi^h(x,y)]/P,$$

for $M_h(x,y)=1$ and $M_l(x,y)=1$, where P is the total number of points that have already been unwrapped using higher threshold γ_h. The final unwrapped phase values within this hole are calculated using the following equation:

$$\Phi_f(x,y) = \begin{cases} \Phi^h(x,y) & M_h(x,y)=1 \\ \Phi_s^l(x,y) - \delta\Phi & M_h(x,y)=0 \text{ and } M_l(x,y)=1 \\ 0 & \text{otherwise} \end{cases}. \quad (10)$$

Once all these holes are filled, the final unwrapped phase map can be obtained, which can be further used for coordinate calculation.

It should be noted that for the hole-filling step, we assume that the traditional phase-unwrapping algorithm can correctly unwrap those points. However, since no phase-unwrapping algorithm is 100% correct, there might be still some errors introduced in these areas. But because the phase unwrapping is performed within holes, it will not propagate beyond their own regions; thus, the incorrectly unwrapped phase will not affect the remaining area.

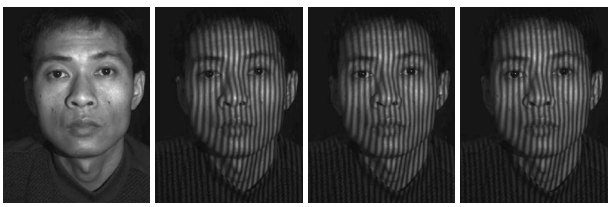

(a) (b) (c) (d)

Fig. 5 Shortest wavelength phase-shifted fringe images. (a) Object; (b) fringe image (0); (c) fringe image ($2\pi/3$); and (d) fringe image ($4\pi/3$).

4 System Setup

The structured light system contains a digital-light-processing (DLP) projector and a charge-coupled device (CCD). The DLP projector used is a Samsung SP-P310MEMX projector with a resolution of 800(H) $\times$600(V). The projection distance range is 0.5 to 2.8 m. The digital micromirror device (DMD) chip used for this projector is 0.55 in. The CCD camera is a digital CCD camera (Pulinx TM6740-CL) with an image resolution of 640$\times$480. The camera sensor pixel size is 7.4 μm(H) $\times$7.4 μm(V). It uses a Computar M0814-MP lens with a focal length of 8 mm at F/1.6 to 16C. The exposure time used for the camera is approximately 8.33 ms. The frame grabber used in this system is a Matrox Solios XCL with CameraLink interface.

5 Experiments

To verify the performance of the proposed framework, we use a six-wavelength phase-shifting algorithm with a longest wavelength of $\lambda_1=600$ and $N=2$. The measured object is a human face, as shown in Fig. 5(a). Figures 5(b)–5(d) show the shortest wavelength fringe images.

Figure 6 shows the phase map of all fringe images without any smoothing. This figure shows that the phase unwrapping is unnecessary for the longest wavelength phase map. It also shows that the phase noise is significant for the background. Since the background does not contain useful information, it is removed by setting a threshold for γ.

Figure 7 shows the final unwrapped phase map after each step. Figure 7(a) shows the phase map without any post-processing using a threshold of $\gamma=0.05$ to remove the background. In the upper half of the image, there are a lot of white spots (noise). Once the Gaussian filter (7$\times$7) is applied, most of these white spots are removed, as shown in Fig. 7(b). However, there is still some noise in this map, such as the white area inside the ellipse of Fig. 7(b). The vertical monotonicity constraint is then applied, and the result is shown in Fig. 7(c). This figure shows that the white spots are drastically less. However, this also generates a lot of small holes (black spots). Last, the hole detection and filling step is applied, and the final result is shown in Fig. 7(d). It can be seen that with the proposed approach, all the phases are smooth, without white or black spots in the major measurement area.

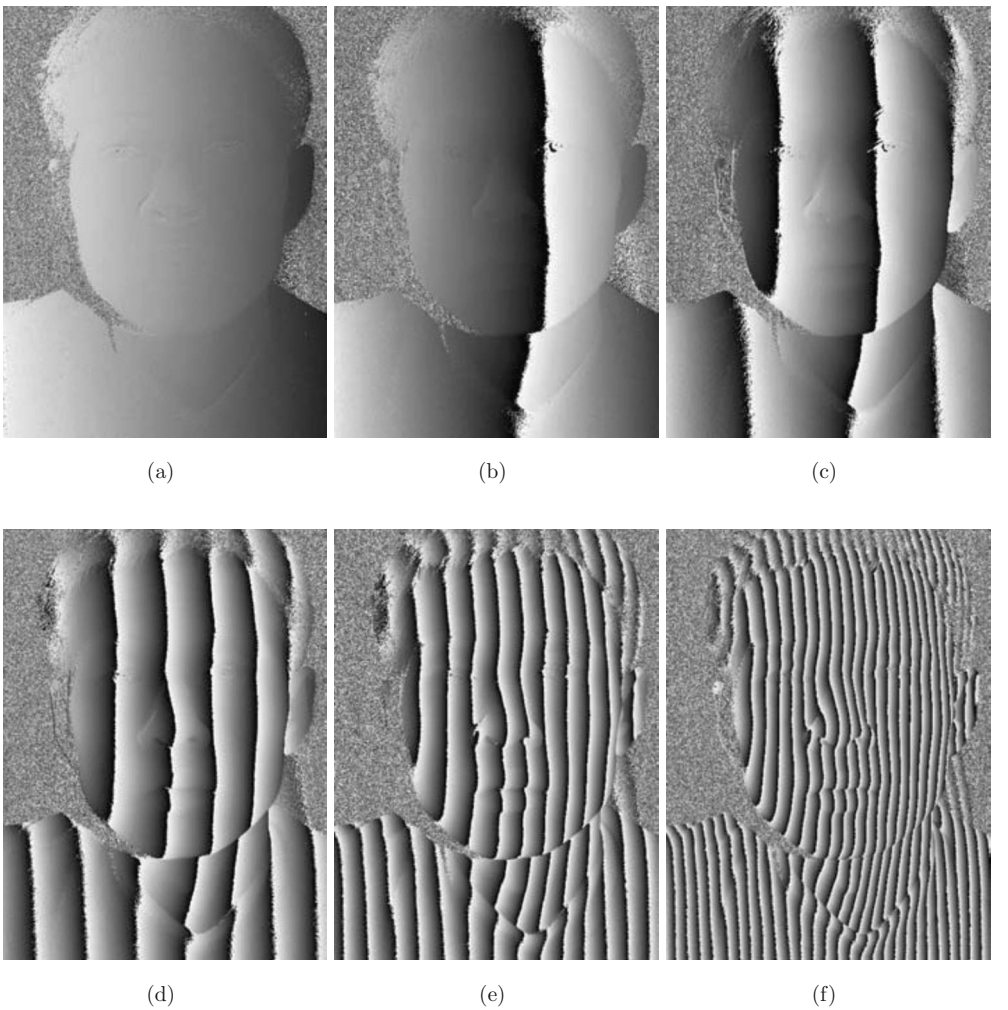

Fig. 6 Phase map computed from each wavelength. (a) $\lambda 1=600$; (b) $\lambda 2=300$; (c) $\lambda 3=150$; (d) $\lambda 4=75$; (e) $\lambda 5=37.5$; and (f) $\lambda 6=18.75$.

For a low threshold, as shown in the previous example, the holes are small. Even bilinear interpolation is sufficient to fill those holes. However, if a larger threshold is used, the holes will be larger, and the bilinear interpolation might be problematic. To verify the performance of our hole-filling algorithm, we reprocessed the same set of fringe images using a much higher threshold, $\gamma_h=0.15$; the phase map before hole filling is shown in Fig. 8(a). It clearly shows that the holes are much larger. We then apply our hole detection and filling step with a lower threshold of $\gamma_l=0.05$ to remove the background. The result is shown in Fig. 8(b). The final phase map is still very smooth. This experiment demonstrated that our hole detection and filling approach performs satisfactorily.

To visualize the 3-D geometric shape of the measurement, we convert the phase to coordinates using the method introduced in Ref. 19. The 3-D geometry of the phase map shown in Fig. 7(d) and Fig. 8(b) are shown in Fig. 9. The first row of this figure shows the 3-D geometry generated from the phase map shown Fig. 7(d) at different viewing angles, and the second row shows the 3-D geometry converted from the phase map shown in Fig. 9. It can be seen that both 3-D geometries are very smooth, with high quality.

As a comparison, we reconstructed the 3-D geometry using a threshold of 0.05 without adopting our proposed framework; the result is shown in Fig. 10. It can be seen that the 3-D geometry has a lot of spikes that are phase

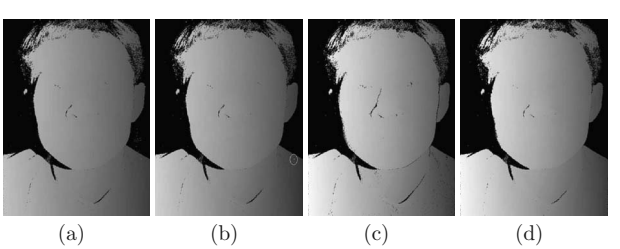

Fig. 7 Phase map after each step with the threshold of $\gamma=0.05$. (a) After applying the γ threshold to be 0.05; (b) after applying the 7×7 Gaussian filter; (c) after removing the bad points using monotonicity constraint; and (d) after detecting and filling holes.

(a) (b)

Fig. 8 Hole filling. (a) Final phase map for higher threshold $\gamma h = 0.15$ without hole filling; (b) phase map after detecting and filling holes using the lower threshold of $\gamma l = 0.05$.

errors caused by the noise. These experiments demonstrate that our proposed framework can significantly alleviate the phase-unwrapping errors caused by the noise.

6 Conclusion

This paper has presented a framework to reduce the phase error for a digital multiple-wavelength phase shifting algorithm. Gaussian filtering is used to reduce the most significant random noise to alleviate its influence on the shorter wavelength phase unwrapping, the monotonic condition is used to further remove those incorrectly unwrapped phase points, the original phase map is unwrapped using the phase-unwrapping integer numbers obtained using the smoothed phase map to preserve the original data, and last holes generated by the too-large threshold used in the previous step are detected and filled. Experiments demonstrate that the proposed framework could significantly reduce the phase errors for such an algorithm.

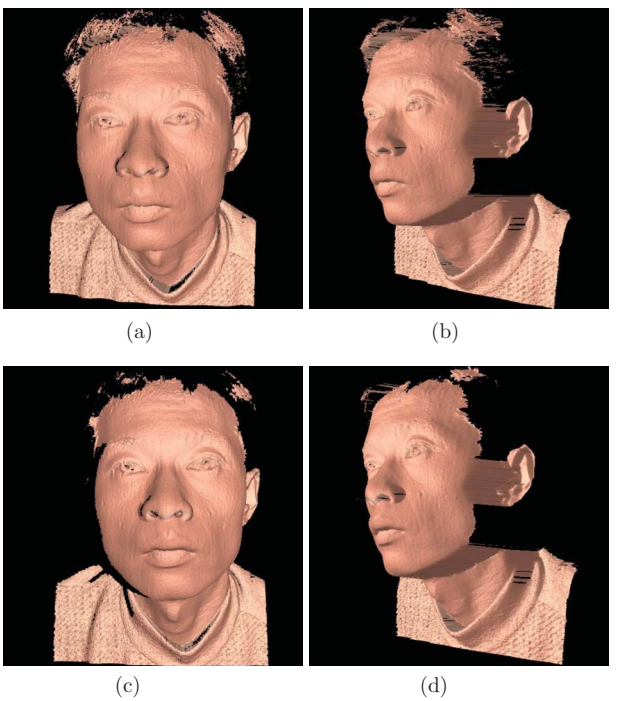

(a) (b)

(c) (d)

Fig. 9 3-D geometric shape of the phase map after coordinate calculations. The first row used 3-D geometry generated from the phase map shown in Fig. 7(d), and the second row used the 3-D geometry converted from the phase map shown in Fig. 8(b).

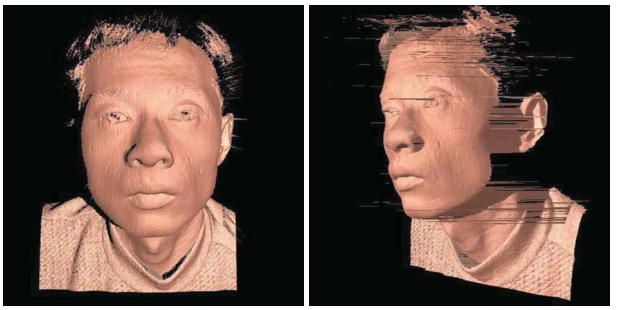

(a) (b)

Fig. 10 3-D result without using the proposed noise reduction framework using threshold $\gamma = 0.05$. (a) Front view; (b) side view.

References

1. C. Polhemus, "Two-wavelength interferometry," *Appl. Opt.* **12**, 2071–2074 (1973).
2. Y.-Y. Cheng and J. C. Wyant, "Two-wavelength phase shifting interferometry," *Appl. Opt.* **23**, 4539–4543 (1984).
3. H. Zhang, W. Chen, and Y. Tan, "Phase-unwrapping algorithm for the measurement of three-dimensional object shapes," *Appl. Opt.* **33**, 4497–4500 (1994).
4. H. O. Saldner and J. M. Huntley, "Profilometry by temporal phase unwrapping and spatial light modulator-based fringe projector," *Opt. Eng.* **36**, 610–615 (1997).
5. J. M. Huntley and H. O. Saldner, "Shape measurement by temporal phase unwrapping: comparison of unwrapping algorithms," *Meas. Sci. Technol.* **8**, 986–992 (1997).
6. Y.-Y. Cheng and J. C. Wyant, "Multiple-wavelength phase shifting interferometry," *Appl. Opt.* **24**, 804–807 (1985).
7. R. Onodera and Y. Ishii, "Two-wavelength interferometry that uses a Fourier-transform method," *Appl. Opt.* **37**, 7988–7994 (1998).
8. K. Creath, "Step height measurement using two-wavelength phase-shifting interferometry," *Appl. Opt.* **26**, 2810–2816 (1987).
9. J. E. Decker, J. R. Miles, A. A. Madej, R. F. Siemsen, K. J. Siemsen, S. D. Bonth, K. Bustraan, S. Temple, and J. R. Pekelsky, "Increasing the range of unambiguity in step-height measurement with multiple-wavelength interferometry-application to absolute long gauge block measurement," *Appl. Opt.* **42**, 5670–5678 (2003).
10. D. S. Mehta, S. K. Dubey, C. Shakher, and M. Takeda, "Two-wavelength Talbot effect and its application for three-dimensional step-height measurement," *Appl. Opt.* **45**, 7602–7609 (2006).
11. M. Roy, C. J. R. Sheppard, G. Cox, and P. Hariharan, "White-light interference microscopy: a way to obtain high lateral resolution over an extended range of heights," *Opt. Express* **14**, 6788–6793 (2006).
12. N. Warnasooriya and M. K. Kim, "LED-based multiwavelength phase imaging interference microscopy," *Opt. Express* **15**, 9239–9247 (2007).
13. D. P. Towers, J. D. C. Jones, and C. E. Towers, "Optimum frequency selection in multifrequency interferometry," *Opt. Lett.* **28**, 1–3 (2003).
14. C. E. Towers, D. P. Towers, and J. D. C. Jones, "Absolute fringe order calculation using optimized multifrequency selection in full-field profilometry," *Opt. Lasers Eng.* **43**, 788–800 (2005).
15. J. M. Huntley and H. O. Saldner, "Temporal phase-unwrapping algorithm for automated interferogram analysis," *Appl. Opt.* **32**, 3047–3052 (1993).
16. H. O. Saldner and J. M. Huntley, "Temporal phase unwrapping: application to surface profiling of discontinuous objects," *Appl. Opt.* **36**, 2770–2775 (1997).
17. D. C. Ghiglia and M. D. Pritt, *Two-Dimensional Phase Unwrapping: Theory, Algorithms, and Software*, John Wiley and Sons, Inc., New

York (1998).
18. S. Zhang, X. Li, and S.-T. Yau, "Multilevel quality-guided phase unwrapping algorithm for real-time three-dimensional shape reconstruction," *Appl. Opt.* **46**, 50–57 (2007).
19. S. Zhang and S.-T. Yau, "High-resolution, real-time 3D absolute coordinate measurement based on a phase-shifting method," *Opt. Express* **45**, 2644–2649 (2006).

Song Zhang is an assistant professor of mechanical engineering, at Iowa State University, where he is also a faculty affiliate of the virtual reality applications center and the human computer interaction graduate program. He received his PhD in mechanical engineering from Stony Brook University in 2005 and worked as a postdoctoral fellow at Harvard University. His major research interests include real-time 3D optical metrology, 3D machine and computer vision, virtual reality, and human computer interaction.